Variance Spectroscopy Studies of Single-Wall Carbon Nanotube Aggregation

Stephen R. Sanchez[†], Sergei M. Bachilo[†], and R. Bruce Weisman,[*,†,‡]*

[†]Department of Chemistry and the Smalley-Curl Institute and [‡]Department of Materials Science and NanoEngineering, Rice University, 6100 Main Street, Houston, Texas 77005

Abstract

Early stages of single-wall carbon nanotube aggregation in aqueous surfactant suspension have been investigated through combined structure-resolved fluorescence and variance spectroscopies. Following the addition of NaCl to destabilize dispersed samples, variance data revealed strong decreases in the concentrations of emitting particles while fluorescence spectra showed only modest changes. This indicates the formation of loose aggregates in which electronic contact between individual nanotubes is too limited to perturb their emission. Variance data showed that the initial formation rates of homo-aggregates (clusters of the same (*n*,*m*) species) increase superlinearly with NaCl concentration. Covariance analysis gave complementary structure-resolved data on emissive hetero-aggregates. For both types of clusters, it is found that the initial aggregation rates correlate with species particle concentrations but show no clear dependence on nanotube structure. Variance spectroscopy can sensitively detect and characterize small loose clusters of carbon nanotube that are not observable by other spectroscopic methods.

Introduction

Aggregation cannot be ignored when working with samples of single-wall carbon nanotubes (SWCNTs). Because of their cylindrical surfaces, SWCNTs have strong tendencies to form parallel bundles bound by van der Waals forces that cumulatively provide substantial cohesive energy. The π-electron systems of nanotubes in such bundles interact significantly, causing efficient excited state energy transfer and spectral distortions that hamper studies of SWCNT intrinsic properties. In fact, the discovery of SWCNT fluorescence and the advent of structure-specific optical spectroscopy were enabled by the introduction of a method for disaggregating bundled samples.[1,2] We also note that the current key research goal of sorting mixtures to obtain structurally pure SWCNTs cannot be achieved using samples with aggregates of different structures.

To date, studies of SWCNT aggregation have been limited by the available experimental tools for detecting and identifying small aggregates. The main current techniques are static light scattering (SLS),[3,4] which can measure particle size and shape parameters, and dynamic light scattering (DLS), which can measure diffusion coefficients and thus hydrodynamic size.[5] SLS has been used in several previous studies related to the stability and aggregation of various carbon nanoparticle systems, including SWCNTs and fullerenes.[6-16] For example, Chen et al. determined through SLS that both acid-treated and Triton X-100 suspended SWCNT aggregates have complex fractal network structures.[17] Khan et al. also used SLS to measure fractal patterns of CoMoCAT SWCNT aggregates formed on exposure to biological media.[12]

Studies using the other light scattering method, DLS, have been mainly focused on environmental aspects of SWCNTs. Several of these have shown that electrolytes can induce the aggregation of SWCNT dispersions, and that the simulation of a natural environment through

addition of organic matter such as humic acid or biomacromolecules can enhance the stability of nanotube dispersions.[10,11,14] Another method with the potential to detect nanotube aggregates is analytical ultracentrifugation.[18] Koh and Cheng applied a combination of optical absorbance and zeta potential measurements to investigate reversible aggregation of aqueous SWCNTs.[13] They determined that electrolyte-induced aggregation is caused by electrostatic interactions following direct binding of counterions to charged SWCNT surfaces. These studies have substantially increased knowledge of the mechanisms and kinetics of SWCNT aggregation. However, conventional optical aggregation probes cannot distinguish among different (*n*,*m*) structural species or detect the earliest stages of aggregation.

Raman spectroscopy has also been found useful for estimating SWCNT aggregation in liquid and solid phases. Heller et al. showed that as nanotubes are electronically perturbed by tight bundling, their Raman excitation profiles red-shift and broaden, thus changing the relative intensities of peaks in the resonance Raman spectrum.[3] The phenomenon is most evident for the RBM peak of (10,2) SWCNTs, which is resonant near 740 nm for individualized nanotubes but shifts to longer wavelengths in bundles. This shift leads to enhanced resonance with 785 nm Raman lasers, greatly intensifying the measured RBM band for bundled samples. This effect is sensitive to strong SWCNT aggregation but does not detect weak clustering, so additional experimental tools are needed for more complete studies. We report here the use of the recently developed method of variance spectroscopy to assess a sample's aggregation state, to sensitively reveal and classify small, weakly bound SWCNT clusters, and to monitor the initial stage of aggregation induced by salt addition.

Approach

SWCNTs in aligned bundles show strong spectral signatures of electronic perturbations: broadened and red-shifted absorption features, decreased overall fluorescence intensity (from quenching by metallic SWCNTs), and redistribution of fluorescence intensity from smaller to larger diameter species (through energy transfer between semiconducting SWCNTs). However, it seems likely that the initial aggregates formed in a SWCNT colloidal dispersion are not bundles of aligned nanotubes, but instead loosely linked clusters containing small numbers of nanotubes oriented at random angles to each other. The small contact areas in such loose aggregates would limit π-system overlap and prevent the stronger interactions evident in bundles. One might then expect the constituent SWCNTs to show nearly the same optical absorption and emission properties as if individualized. The first aggregates formed would be pairs of nanotubes, which might contain the same or different (*n*,*m*) species (homo-aggregates or hetero-aggregates). We will refer to clustered pairs of the same semiconducting SWCNT species as emissive dimers, and pairs with different semiconducting SWCNT species as emissive complexes.

Although neither emissive dimers nor emissive complexes can be detected in conventional absorption or emission spectra, they can be observed and characterized with variance spectroscopy.[19] Variance spectroscopy is a recently developed fluorescence technique that can recover homogeneous spectra of subpopulations in heterogeneous nanoparticle dispersions and measure the particle concentrations of different emitters.[19,20] The formation of an emissive dimer converts two independent SWCNTs into one dimeric cluster emitting at the same wavelength. This event leaves total fluorescence intensity unchanged but reduces the number of spatially independent emissive particles from two to one. It is therefore evident as a decrease in

particle concentration in variance analysis, or alternatively through skewness analysis of the third moment of fluorescence intensity distributions.[21] In the other binary clustering case, formation of an emissive complex from two s-SWCNTs of different species does not change the apparent particle concentration of either species in variance spectra, because the cluster is counted as one particle of each. However, a covariance analysis of the variance data will reveal the emissive complex through correlated fluctuations at the two different emission wavelengths. Thus, we use variance spectroscopy to detect the most subtle aggregation step, the loose clustering of just two s-SWCNTs, and to distinguish homo- from hetero-aggregates.

Materials and Methods

Sample preparation. Approximately 3 mg of raw SWCNT material (Rice University HiPco reactor, batch 195.1) or raw CoMoCAT SWCNTs (SouthWest NanoTechnologies grade SG65i) was suspended in 10 mL of 0.5% sodium tridecylbenzenesulfonate (STBS) using 30 min of bath sonication (Sharpertek Stamina XP) followed by 20 min of tip sonication at 5 W (3 mm tip, Branson Digital Sonifier). The suspensions were then ultracentrifuged at 268,000 g for 4 h (Beckman Optima MAX-130k) to remove bundles and impurities. We diluted supernatants with 0.5% STBS before use to give stock solutions with final SWCNT mass concentrations of approximately 1 mg/L. Aggregation was induced by adding measured volumes of 1 M aqueous NaCl.

Bulk sample characterization. We measured bulk fluorescence and absorption spectra using a prototype NS2 or NS3 NanoSpectralyzer (Applied NanoFluorescence, LLC), allowing selected fluorescence excitation at 638, 642, 659, and 784 nm. Time-sequenced fluorescence spectra were acquired only with 642 nm laser excitation. We determined the length distribution of the HiPco SWCNT sample used for variance experiments by the Length Analysis by

Nanotube Diffusion (LAND) method.[22,23] In this technique, short-wave IR videomicroscopy is used to track the 2-D Brownian motion of individual SWCNTs and deduce lengths from their diffusion coefficients. We observed samples using a Nikon TE-2000U inverted microscope equipped with a Nikon Plan Apo 60x/1.27 NA water-immersion objective. SWCNTs were excited using a continuous wave Ti:sapphire laser (Del Mar Photonics) emitting 160 mW at 840 nm. We placed a quarter-wave retardation plate in the excitation beam to obtain circular polarization and minimize fluorescence blinking from nanotube rotational diffusion.[24] The E_{11} emission from (6,5) SWCNTs was spectrally selected using a pair of filters (950 nm long-pass and 1000 nm short-pass) and imaged with 100 ms exposure times by an InGaAs camera (Roper Scientific 2D-OMA V) cooled to -95°C. The sample was diluted with 1% aqueous sodium deoxycholate to minimize adhesion to the glass cell surfaces. Also, in order to more easily track shorter SWCNTs, we increased the sample viscosity to ~30 mPa·s by adding sorbitol.

Variance Spectroscopy. Variance spectroscopy involves the capture of spectra from many equivalent small volumes in dilute dispersions of heterogeneous nanoparticles. The spectra are then statistically analyzed to obtain first and second moments (mean and variance) at each wavelength. Because this method is spectrally resolved, it provides (*n*,*m*)-specific information for SWCNT samples. Our custom-built apparatus was similar to that reported previously.[20] In brief, liquid samples were loaded into a demountable cuvette with 100 μm path length (Precision Cells Type 20), which was placed in a custom holder positioned in three dimensions by a set of computer-controlled translation stages (PI model M-111.12S). A 660 nm diode laser (Power Technology, Inc.) was used to excite the sample. Two short pass filters (875 and 1100 nm, Edmund Optics) removed stray short-wave infrared emission from the excitation path, and a quarter-wave retardation plate (Thorlabs) converted the beam to circular polarization. Finally,

the beam passed through the hole of a drilled reflective beam coupler to a fused silica aspheric lens (EFL=8.0 mm, NA=0.63, Edmund Optics). This lens was used for both excitation focusing and emission collection in epifluorescence geometry. Sample emission was reflected by the coupler, directed through a 850 nm long pass filter (Newport Corp.), and focused by a fiber collimator (f=11 mm, Thorlabs) into a multimode optical fiber (300 μm core diameter, NA=0.39, Thorlabs). The optical fiber was coupled to the input of a SWIR spectrometer (B&WTek Sol 1.7). Spectra from 840 to 1650 nm were captured by the spectrometer's thermoelectrically cooled 512 channel InGaAs detector array and transferred to a Windows-based computer for analysis by custom LabView software. The cell motion sequence and details of the variance data analysis are described in Supporting Information. Calibration of the effective probed volume was performed using an independently determined value of the (6,5) E_{11} absolute absorption cross section.[25,26] Each variance data set comprised 3000 spectra acquired during a 30 min period. Initial acquisitions began 5 min after NaCl addition to allow for sample preparation and loading. Data in kinetic plots have time coordinates showing the mid-point of the data acquisition period. Abundance values deduced from variance data have estimated relative uncertainties of 3 to 8%.

Results and Discussion

Effects of aggregation on fluorescence spectra. SWCNT aggregation is suppressed in surfactants that provide robust coverage of nanotube surfaces, and enabled in surfactants that give less stable surface coverage because of low affinities or low concentrations. For this study, we therefore chose a relatively poor nanotube surfactant, 0.5% aqueous STBS, that allowed NaCl-induced aggregation on time scales accessible to our experimental method. Although this particular surfactant is not commonly used in SWCNT research, we think that our qualitative

findings on aggregation processes will have general validity. Duque et al.[27] reported that adding low concentrations of NaCl to SWCNTs dispersed in 1% SDS increased the fluorescence intensity of small diameter species through surfactant reorganization and saturation. However, at NaCl concentrations above 60 mM they instead observed quenching. As shown in Figures 1a and 1b, we similarly found intensity decreases for all emission features in HiPco and CoMoCAT sample dispersions after exposure to 100 mM NaCl. Figures 1c and 1d show plots of these time profiles for several (*n*,*m*) emission peaks. As discussed above, weak nanotube clustering should not change emission intensities, so the observed decreases are presumed to arise mainly from short-ranged interactions in tight bundles. The data suggest more than one effect. We attribute the general decreases to quenching by metallic SWCNTs bundled with semiconducting species. This quenching through bundling seems fastest for larger diameter nanotubes, possibly because their micellar coatings are more disrupted by the added salt. The spectral intensity pattern also suggests concurrent energy transfer from nanotubes with larger band gaps to others with smaller band gaps. This accelerates the loss of emission from donor species such as (8,3) and (6,5) and slows the loss of emission from acceptor species such as (7,6) and (8,6).

To monitor the environment of the emissive particles, we also determined peak positions for many (*n*,*m*) species by fitting the mean emission spectra as a superposition of Voigt functions (see Supporting Information). In a previous study, McDonald et al. investigated spectral peak shifts resulting from aggregation induced by surfactant dilution.[28] They found that when such aggregation was strong enough to substantially reduce the emission intensity, spectral shifts ranged between -1 and -5 meV. This effect was interpreted as the result of water quenching of nanotubes with reduced surfactant coverage. In this work, we observed spectral shifts smaller than 1 meV under conditions giving to up to 20% loss of intensity and 70% loss of abundance

(see Figure S15). Our results may therefore be viewed as reflecting early stage processes with relatively unperturbed surfactant coatings.

Monitoring homo-aggregates through variance spectroscopy. To probe for more subtle aggregation induced by lower concentrations of NaCl, we measured variance spectra on SWCNT dispersions at different times after salt exposure. Each variance measurement gave mean and variance spectra, $\overline{I}(\lambda)$ and $\sigma^2(\lambda)$, from which we obtained the number of particles, N, in the probed volume that emit at wavelength λ using the expression $N = \overline{I}^2(\lambda)/\sigma^2(\lambda)$. Figure 2 shows the mean and variance spectra for a dispersed sample before and 320 min after exposure to 30 mM NaCl. Peaks in the mean spectrum (top frame) decreased by less than 5%, through the mechanisms discussed above, while peaks in the variance spectrum (bottom frame) *increased* by 0 to 40%. These variance increases reveal reductions in the number of emissive particles caused by homo-aggregation. The large increase in (7,6) variance is explained by the high abundance of this species in the sample, which allows a high rate of encounters between individual (7,6) nanotubes and rapid formation of homo-aggregates. By contrast, (8,3) nanotubes are far less abundant and show almost no evidence of homo-aggregation under these experimental conditions (the (8,3) emission is intense because its E_{22} transition is nearly resonant with the 660 nm excitation wavelength). Comparison of the top and bottom frames in Figure 2 shows that the two types of spectra are sensitive to different aggregation processes and that the variance increases are strongly dominated by homo-aggregation rather than quenching of emissive particles by energy transfer to metallic species.

Figures 3a,b present kinetic plots of (*n*,*m*)-resolved emission intensity and deduced particle abundance for the sample of Figure 2 (30 mM NaCl). There are significant, species-

dependent drops in particle abundance while species-resolved emission intensities show much smaller changes. This reveals the formation of loose homo-aggregates.Figures 3c,d and 3e,f plot the time dependent changes in emission intensity and particle abundance for (8,3) and (7,6) SWCNTs in the sample after exposure to NaCl concentrations ranging from 30 to 120 mM. We show data for these two species because (8,3) was the least abundant and (7,6) was the most abundant in our sample. Although the relative changes in emission intensities are similar for these species, the relative abundance drops much more sharply for (7,6) than for (8,3) at all salt concentrations. This is explained by the fact that our measured particle abundances decrease only when nanotubes of the same (*n*,*m*) species cluster together. The changes in abundance should therefore be most rapid for the species with the highest particle concentration, which has the most frequent nanotube-nanotube encounters. Figures 3d,f also show that the rate of relative abundance loss increases strongly with increasing salt concentration (see Supporting Information for details). Higher salt concentrations reduce the electrostatic repulsion between surfactant-coated nanotubes by screening surface charges.[29] After several hours of exposure to salt concentrations near 100 mM, the relative abundances of all species in our samples decreased to only 10-20% of their initial values. It is likely that the sample contains a highly polydisperse size distribution of aggregates under these conditions, with very few individualized SWCNTs remaining in the sample.[30]

A simplified analysis of early homo-aggregation considers only the clustering of pairs of nanotubes, which converts two observed particles to one. This process can be modeled by the following integrated second-order rate law:

$$N_t^{(n,m)} = \frac{N_0^{(n,m)}}{2}\left(\frac{2 + N_0^{(n,m)} k_a^{(n,m)} t}{1 + N_0^{(n,m)} k_a^{(n,m)} t}\right) \quad (1)$$

Here $N_t^{(n,m)}$ is the particle concentration of a specific (*n*,*m*) species at time *t* after salt addition, $N_0^{(n,m)}$ is the initial particle concentration of the species, and $k_a^{(n,m)}$ is the (*n*,*m*)-specific homo-aggregation rate constant. Because the coarse time resolution of our variance measurements allowed few data points within the validity regime of eq 1, it was not possible to meaningfully fit most of the abundance traces to the equation. Instead, for each plot of normalized abundance vs time, we estimated the initial slope and divided by the initial abundance to obtain a parameter proportional to the second-order homoaggregation rate constant $k_a^{(n,m)}$. We performed this analysis for six (*n*,*m*) species at three NaCl concentrations to give the results plotted vs NaCl concentration in Figure 4. Although the data show considerable scatter, the average aggregation rate constants increase superlinearly with NaCl concentration. In addition, no clear dependence on (*n*,*m*) is evident within the uncertainty of the data. This is consistent with the expectation that attachment efficiency, a parameter related to the number of encounters needed to produce an aggregate, is similar for the different species.[5]

Monitoring hetero-aggregates through covariance analysis. At the same time that SWCNTs of the same type are forming homo-aggregates that we track by decreases in particle abundance, SWCNTs of different types must be loosely clustering to form hetero-aggregates. To probe for those emissive complexes, we analyze variance data to construct a covariance matrix showing correlations between emission fluctuations at different wavelengths. No additional data collection is needed for this analysis. Positive correlations arise from the presence of emissive clusters containing different semiconducting (*n*,*m*) species, because physical linkage of the emission centers synchronizes the statistical intensity fluctuations at their separate E_{11} fluorescence wavelengths. Figure 5 shows contour plots of covariance matrices measured on a SWCNT dispersion before and 320 min after exposure to 30 mM NaCl. (Additional covariance

plots are shown in Supporting Information Figures S9-S12.) A diagonal trace from lower left to upper right through this plot gives the variance spectrum (as in Figure 2b), with all diagonal features representing individualized SWCNTs or homo-aggregates. Off-diagonal features represent emissive complexes that emit fluorescence at both the x- and y-coordinate wavelengths. Note that covariance plots have reflection symmetry relative to the diagonal. A horizontal or vertical trace through an (*n*,*m*) peak gives a covariance spectrum showing correlations of all other wavelengths with that (*n*,*m*) emission peak.

In Figure 6a we plot covariance spectra through the (7,6) peak for the sample of Figure 5 at 0, 128, and 320 min after exposure to 30 mM NaCl. These traces have been normalized to the 1125 nm peak of (7,6), which equals its variance and increases with time as homo-aggregation reduces the (7,6) particle abundance. The off-diagonal covariance features give peaks in this plot at wavelengths other than 1125 nm. These are seen to grow steadily with time, indicating the formation of emissive complexes containing (7,6) clustered with another species. Two factors may contribute to the presence of weak off-diagonal features in the time zero trace. First, the initial dispersion might have contained some small loose aggregates that were not efficiently removed by the centrifugation processing. It is also likely that some aggregates formed during the ca. 25 min after salt addition needed to transfer the sample to the variance cell and acquire the first set of 3000 spectra.

To quantify the degree of hetero-aggregation, we calculated scaled Pearson correlation coefficients (normalized covariances) between pairs of the resolvable SWCNT species at various times. The following expression describes the fraction of the SWCNTs emitting at wavelength λ_j that are clustered with a nanotube emitting at λ_k:

$$\rho\left(\lambda_j,\lambda_k\right)=\sqrt{\frac{n_j^0}{n_k^0}}\ \frac{\mathrm{cov}\left(\lambda_j,\lambda_k\right)}{\sigma\left(\lambda_j\right)\sigma\left(\lambda_k\right)}\ . \tag{2}$$

Here *cov* is the statistical covariance function and the factor $\sqrt{n_j^0/n_k^0}$ accounts for differences in the initial abundances of the two species.[19] We further performed numerical simulations to correct for correlations caused by spectral overlap instead of clustering (see Supporting Information). By applying this analysis to a time series of measurements made during aggregation, we deduced kinetics for the fractions of (7,6)-emissive particles that clustered with the five other easily resolved (*n*,*m*) species. Figure 6b shows these kinetics results, with linear fits through the data. The slopes in Figure 6b are approximately proportional to species particle abundance (see Supporting Information, Figure S16), reflecting the relative rates at which (7,6) SWCNTs encounter other species of nanotubes. The initial correlation values also tend to increase with particle abundances, which are smallest for (8,3) and greatest for (8,6). Note that the fractions plotted in Figure 6b can sum to values greater than one as clusters grow to include multiple nanotubes.

To supplement the calculation of the scaled correlation coefficients, we have estimated cluster compositions using a new analysis method based on covariance spectra (for details, see the last section of Supporting Information). The underlying idea is that a horizontal slice of the 2D covariance map passing through a given diagonal peak such as (7,6) shows off-diagonal peaks that are the emission components from other (*n*,*m*) species clustered with (7,6). The magnitude of each off-diagonal peak can be converted to the number of contributing (*n*,*m*) particles by using separately determined values for mean emission per particle. Comparing this to the number of (7,6) particles then gives the desired average number of (*n*,*m*) nanotubes clustered per (7,6).

We performed this analysis on the final (t = 320 min) and initial data sets after sample exposure to 30 mM NaCl. Figure 7 shows those covariance spectra and emission efficiency spectra. Using their deconvolutions into (n,m) components, we deduced that (7,6)-emissive particles had clustered with approximately 1 or 2 other nanotubes during this period, with no clear dependence on diameter of the partner SWCNT (see Figure S17). This result is consistent with our finding from correlation analysis that the (7,6) species does not show (n,m) selectivity in early stages of salt-induced hetero-aggregation.

Conclusions

We have combined fluorescence and variance spectroscopies to gain new insights into the aggregation of SWCNTs in aqueous surfactant suspension. After adding NaCl to stable dispersions, we observed mild, structure-dependent decreases in fluorescence intensities consistent with quenching from contact with metallic nanotubes and energy transfer between semiconducting species. At the same time, variance data revealed sharper decreases in the concentrations of emitting particles. The combined observations imply the formation of loose aggregates in which the individual nanotubes retain their unperturbed emissive properties. Further analysis of variance data showed that the average rates of initial homo-aggregation (clustering of the same (n,m) species) increase superlinearly with NaCl concentration. Covariance analysis allowed structure-resolved observation of emissive hetero-aggregates. Consistent with the homo-aggregation results, it was found that the initial clustering rates correlate with species particle concentrations, without (n,m) selectivity. This study demonstrates that variance spectroscopy can sensitively quantify the formation of carbon nanotube clusters that are not observable by other spectroscopic methods. The results should be relevant to

biomedical and environmental systems in which SWCNTs are suspended in high ionic strength media.

Associated Content

Supporting Information

The Supporting Information is available free of charge on the ACS Publications website at DOI: 10.1021/acs.jpcc.xxxxxxx.

Variance data acquisition and data analysis, correlation simulations for spectral overlap correction, sample fluorescence and absorption spectra, sample length distribution, kinetic plots of fluorescence intensity and particle abundance, covariance matrix contour plots, spectral fitting details, emission peak shifts, covariance growth vs particle abundance, hetero-aggregate growth vs SWCNT diameter, expressions for deducing cluster compositions from off-diagonal covariance peaks.

Author Information

Corresponding Author

E-mail: weisman@rice.edu. Tel: 713-3483709. Fax: 713-348-5155.

Notes

The authors declare the following competing financial interest(s): R.B.W. has a financial interest in Applied NanoFluorescence, LLC, which manufactures one of the instruments used in this study.

Acknowledgements

This research was supported by grants from the National Science Foundation (CHE-1409698) and the Welch Foundation (C-0807). S.R.S is grateful to the National Science Foundation for support through an AGEP-GRS award (CHE-1401269). The authors also thank C.-W. Lin for assistance with LabVIEW programming and for useful discussions on apparatus construction.

References

(1) O'Connell, M. J.; Bachilo, S. M.; Huffman, C. B.; Moore, V.; Strano, M. S.; Haroz, E.; Rialon, K.; Boul, P. J.; Noon, W. H.; Kittrell, C., et al. Band-Gap Fluorescence from Individual Single-Walled Carbon Nanotubes. *Science* **2002,** *297*, 593-596.

(2) Bachilo, S. M.; Strano, M. S.; Kittrell, C.; Hauge, R. H.; Smalley, R. E.; Weisman, R. B. Structure-Assigned Optical Spectra of Single-Walled Carbon Nanotubes. *Science* **2002,** *298*, 2361-2366.

(3) Heller, D. A.; Barone, P. W.; Swanson, J. P.; Mayrhofer, R. M.; Strano, M. S. Using Raman Spectroscopy to Elucidate the Aggregation State of Single-Walled Carbon Nanotubes. *J. Phys. Chem. B* **2004,** *108*, 6905-6909.

(4) O'Connell, M. J.; Sivaram, S.; Doorn, S. K. Near-Infrared Resonance Raman Excitation Profile Studies of Single-Walled Carbon Nanotube Intertube Interactions: A Direct Comparison of Bundled and Individually Dispersed Hipco Nanotubes. *Phys. Rev. B* **2004,** *69*, 235415.

(5) Elimelech, M.; Gregory, J.; Jia, X., *Particle Deposition and Aggregation: Measurement, Modelling and Simulation;* Butterworth-Heinemann: 2013.

(6) Bouchard, D.; Zhang, W.; Powell, T.; Rattanaudompol, U. Aggregation Kinetics and Transport of Single-Walled Carbon Nanotubes at Low Surfactant Concentrations. *Environ. Sci. Technol.* **2012,** *46*, 4458-4465.

(7) Chen, K. L.; Elimelech, M. Aggregation and Deposition Kinetics of Fullerene (C60) Nanoparticles. *Langmuir* **2006,** *22*, 10994-11001.

(8) Chen, K. L.; Elimelech, M. Influence of Humic Acid on the Aggregation Kinetics of Fullerene (C60) Nanoparticles in Monovalent and Divalent Electrolyte Solutions. *J. Colloid Interface Sci.* **2007,** *309*, 126-134.

(9) Forney, M. W.; Anderson, J. S.; Ameen, A. L.; Poler, J. C. Aggregation Kinetics of Single-Walled Carbon Nanotubes in Nonaqueous Solvents: Critical Coagulation Concentrations and Transient Dispersion Stability. *J. Phys. Chem. C* **2011,** *115*, 23267-23272.

(10) Ju, L.; Zhang, W.; Wang, X.; Hu, J.; Zhang, Y. Aggregation Kinetics of Sdbs-Dispersed Carbon Nanotubes in Different Aqueous Suspensions. *Colloids and Surfaces A: Physicochemical and Engineering Aspects* **2012,** *409*, 159-166.

(11) Khan, I. A.; Afrooz, A. R. M. N.; Flora, J. R. V.; Schierz, P. A.; Ferguson, P. L.; Sabo-Attwood, T.; Saleh, N. B. Chirality Affects Aggregation Kinetics of Single-Walled Carbon Nanotubes. *Environ. Sci. Technol.* **2013,** *47*, 1844-1852.

(12) Khan, I. A.; Aich, N.; Afrooz, A. R. M. N.; Flora, J. R. V.; Schierz, P. A.; Ferguson, P. L.; Sabo-Attwood, T.; Saleh, N. B. Fractal Structures of Single-Walled Carbon Nanotubes in Biologically Relevant Conditions: Role of Chirality Vs. Media Conditions. *Chemosphere* **2013,** *93*, 1997-2003.

(13) Koh, B.; Cheng, W. Mechanisms of Carbon Nanotube Aggregation and the Reversion of Carbon Nanotube Aggregates in Aqueous Medium. *Langmuir* **2014,** *30*, 10899-10909.
(14) Saleh, N. B.; Pfefferle, L. D.; Elimelech, M. Influence of Biomacromolecules and Humic Acid on the Aggregation Kinetics of Single-Walled Carbon Nanotubes. *Environ. Sci. Technol.* **2010,** *44*, 2412-2418.
(15) Saleh, N. B.; Pfefferle, L. D.; Elimelech, M. Aggregation Kinetics of Multiwalled Carbon Nanotubes in Aquatic Systems: Measurements and Environmental Implications. *Environ. Sci. Technol.* **2008,** *42*, 7963-7969.
(16) Yi, P.; Chen, K. L. Influence of Surface Oxidation on the Aggregation and Deposition Kinetics of Multiwalled Carbon Nanotubes in Monovalent and Divalent Electrolytes. *Langmuir* **2011,** *27*, 3588-3599.
(17) Chen, Q.; Saltiel, C.; Manickavasagam, S.; Schadler, L. S.; Siegel, R. W.; Yang, H. Aggregation Behavior of Single-Walled Carbon Nanotubes in Dilute Aqueous Suspension. *J. Colloid Interface Sci.* **2004,** *280*, 91-97.
(18) Silvera Batista, C. A.; Zheng, M.; Khripin, C. Y.; Tu, X.; Fagan, J. A. Rod Hydrodynamics and Length Distributions of Single-Wall Carbon Nanotubes Using Analytical Ultracentrifugation. *Langmuir* **2014,** *30*, 4895-4904.
(19) Streit, J. K.; Bachilo, S. M.; Sanchez, S. R.; Lin, C.-W.; Weisman, R. B. Variance Spectroscopy. *J. Phys. Chem. Lett.* **2015,** *6*, 3976-3981.
(20) Sanchez, S. R.; Bachilo, S. M.; Kadria-Vili, Y.; Lin, C.-W.; Weisman, R. B. (*N,M*)-Specific Absorption Cross Sections of Single-Walled Carbon Nanotubes Measured by Variance Spectroscopy. *Nano Lett.* **2016,** *16*, 6903-6909.
(21) Sanchez, S. R.; Bachilo, S. M.; Kadria-Vili, Y.; Weisman, R. B. Skewness Analysis in Variance Spectroscopy Measures Nanoparticle Individualization. *J. Phys. Chem. Lett.* **2017,** *8*, 2924-2929.
(22) Streit, J. K.; Bachilo, S. M.; Naumov, A. V.; Khripin, C.; Zheng, M.; Weisman, R. B. Measuring Single-Walled Carbon Nanotube Length Distributions from Diffusional Trajectories. *ACS Nano* **2012,** *6*, 8424-8431.
(23) Tsyboulski, D. A.; Bachilo, S. M.; Weisman, R. B. Versatile Visualization of Individual Single-Walled Carbon Nanotubes with near-Infrared Fluorescence Microscopy. *Nano Lett.* **2005,** *5*, 975-979.
(24) Tsyboulski, D. A.; Bachilo, S. M.; Kolomeisky, A. B.; Weisman, R. B. Translational and Rotational Dynamics of Individual Single-Walled Carbon Nanotubes in Aqueous Suspension. *ACS Nano* **2008,** *2*, 1770-1776.
(25) Streit, J. K.; Bachilo, S. M.; Ghosh, S.; Lin, C.-W.; Weisman, R. B. Directly Measured Optical Absorption Cross Sections for Structure-Selected Single-Walled Carbon Nanotubes. *Nano Lett.* **2014,** *14*, 1530-1536.
(26) Sanchez, S. R.; Bachilo, S. M.; Kadria-Vili, Y.; Lin, C.-W.; Weisman, R. B. (*N,M*)-Specific Absorption Cross Sections of Single-Walled Carbon Nanotubes Measured by Variance Spectroscopy. *Nano Lett.* **2016,** *16*, 6903-6909.
(27) Duque, J. G.; Densmore, C. G.; Doorn, S. K. Saturation of Surfactant Structure at the Single-Walled Carbon Nanotube Surface. *J. Am. Chem. Soc.* **2010,** *132*, 16165-16175.
(28) McDonald, T. J.; Engtrakul, C.; Jones, M.; Rumbles, G.; Heben, M. J. Kinetics of Pl Quenching During Single-Walled Carbon Nanotube Rebundling and Diameter-Dependent Surfactant Interactions. *J. Phys. Chem. B* **2006,** *110*, 25339-25346.
(29) Niyogi, S.; Boukhalfa, S.; Chikkannanavar, S. B.; McDonald, T. J.; Heben, M. J.; Doorn, S. K. Selective Aggregation of Single-Walled Carbon Nanotubes Via Salt Addition. *J. Am. Chem. Soc.* **2007,** *129*, 1898-1899.
(30) Ameen, A. A.; Giordano, A. N.; Alston, J. R.; Forney, M. W.; Herring, N. P.; Kobayashi, S.; Ridlen, S. G.; Subaran, S. S.; Younts, T. J.; Poler, J. C. Aggregation Kinetics of Single-Walled

Carbon Nanotubes Investigated Using Mechanically Wrapped Multinuclear Complexes: Probing the Tube-Tube Repulsive Barrier. *Phys. Chem. Chem. Phys.* **2014,** *16*, 5855-5865.

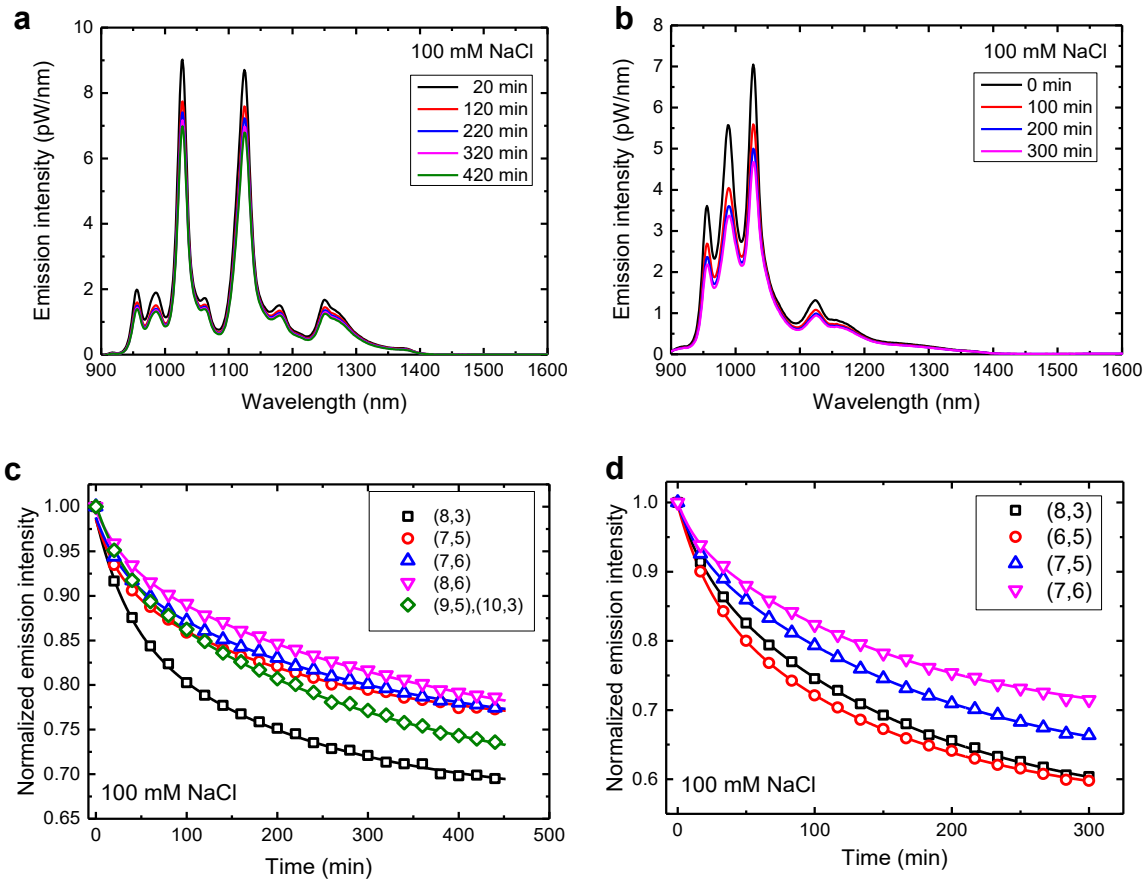

Figure 1. (a) Emission spectra of a HiPco SWCNT sample dispersed in aqueous 0.5% STBS measured over the first 400 min of exposure to 100 mM NaCl. Excitation was at 642 nm. **(b)** Emission spectra of a CoMoCAT SG65i SWCNT sample dispersed sample dispersed in aqueous 0.5% STBS measured over the first 300 min of exposure to 100 mM NaCl. **(c)** Time-dependent normalized intensities of five emission peaks in frame (a) (HiPco sample) assigned to the (*n*,*m*) species shown in the legend. **(d)** Time-dependent normalized intensities of four emission peaks in frame (b) (CoMoCAT SG65i sample) assigned to the (*n*,*m*) species shown in the legend.

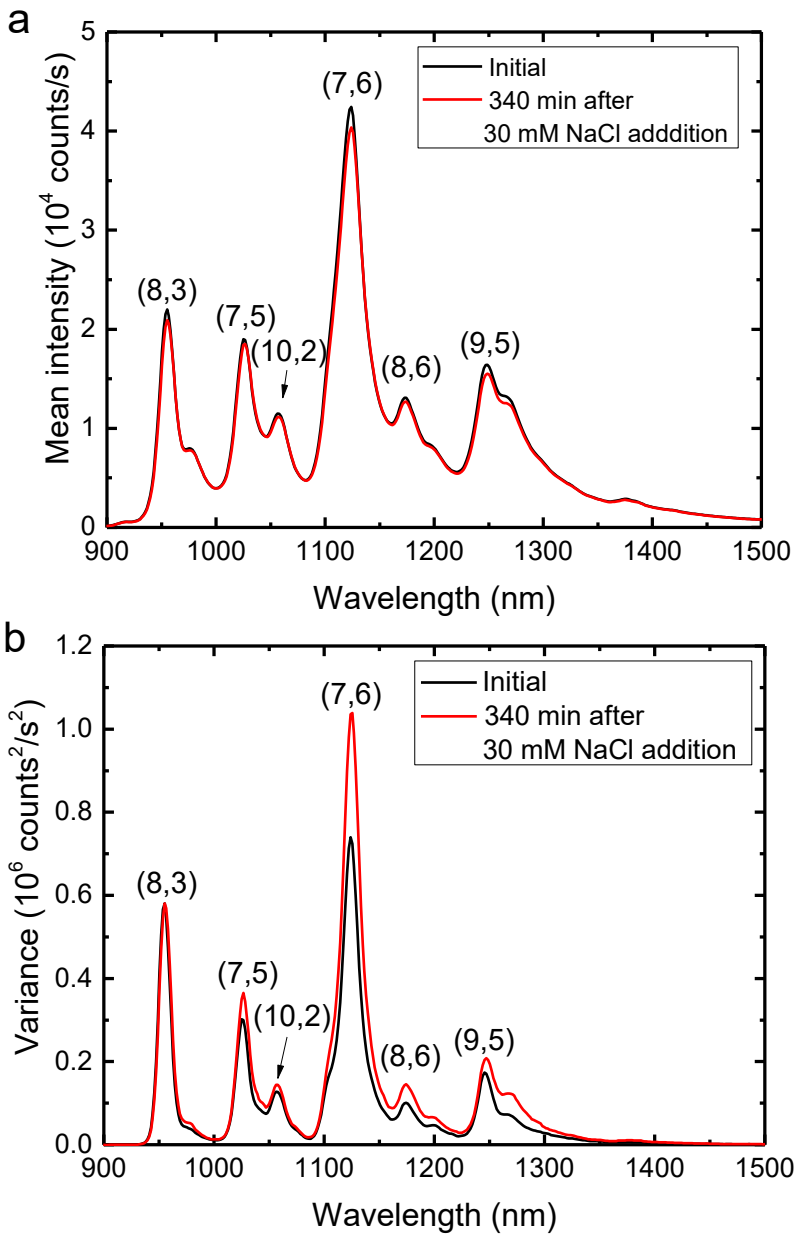

Figure 2. Changes in the mean spectrum **(a)** and variance spectrum **(b)** from 340 min of exposure to 30 mM NaCl for a HiPco SWCNT sample dispersed in aqueous 0.5% STBS. The initial traces (black curves) were calculated from the first set of 3000 spectra, measured 5 to 35 min after NaCl addition. The final traces (red curves) were calculated from a set of spectra measured 325 to 355 min after salt addition. Labels mark the six resolvable (*n*,*m*) species tracked in this study.

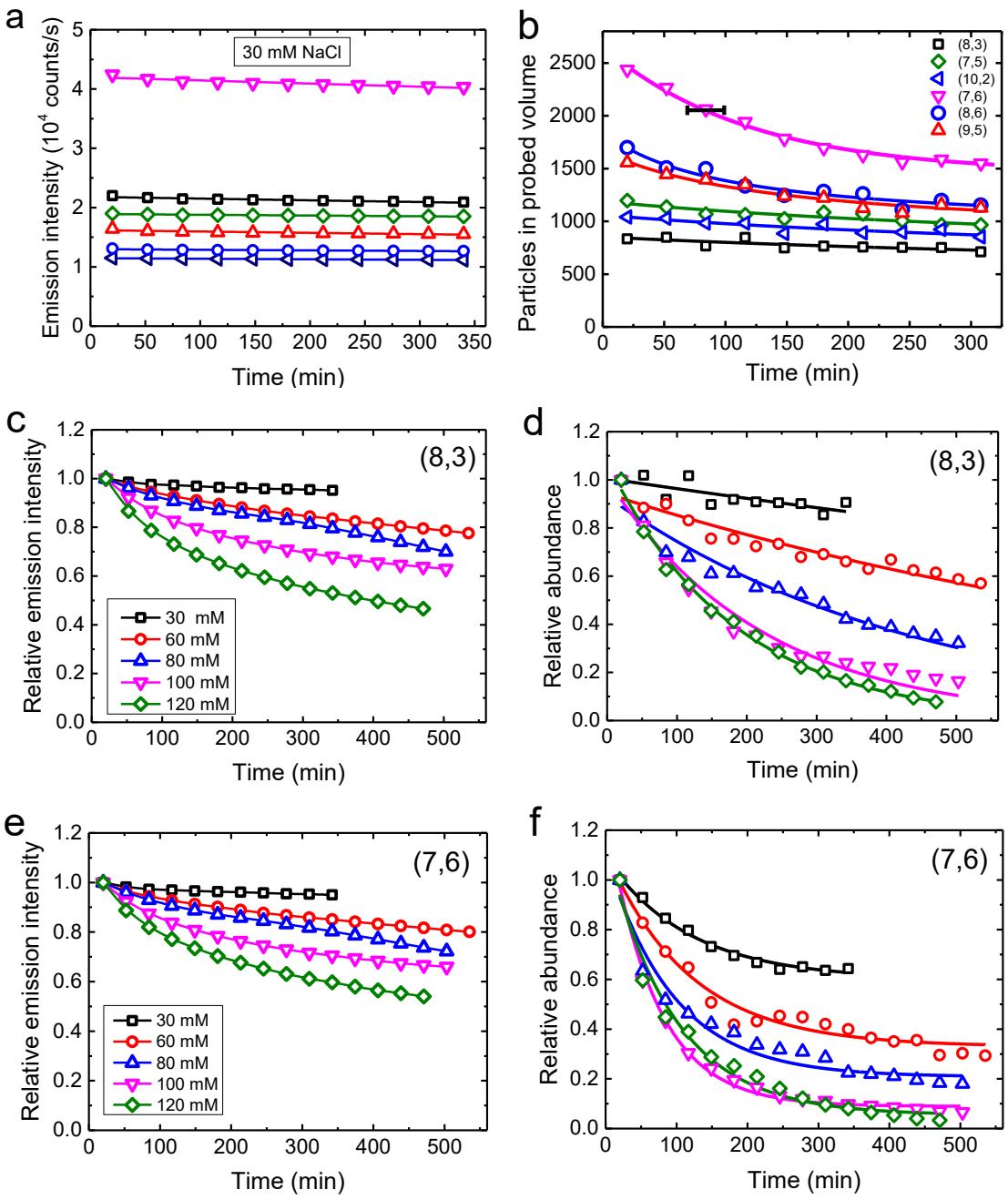

Figure 3. Kinetics of structure-resolved emission intensity **(a)** and relative particle abundance **(b)** for a HiPco dispersion exposed to 30 mM NaCl (See legend for (*n*,*m*) species symbol codes. The horizontal bar in the top trace at t = 50 min marks the measurement duration for each data point.) Frame **(c)** shows kinetics of relative emission intensity and **(d)** shows relative particle abundance for (8,3) SWCNTs exposed to NaCl concentrations from 30 to 120 mM (See legend for concentration symbol codes). Frame **(e)** shows kinetics of relative emission intensity and **(f)** shows relative particle abundance for (7,6) SWCNTs exposed to NaCl concentrations from 30 to 120 mM. In this unsorted sample, (8,3) is the least abundant species and (7,6) is the most abundant. Plots (c) through (f) are normalized to the first measurement after salt addition. Solid curves are guides to the eye.

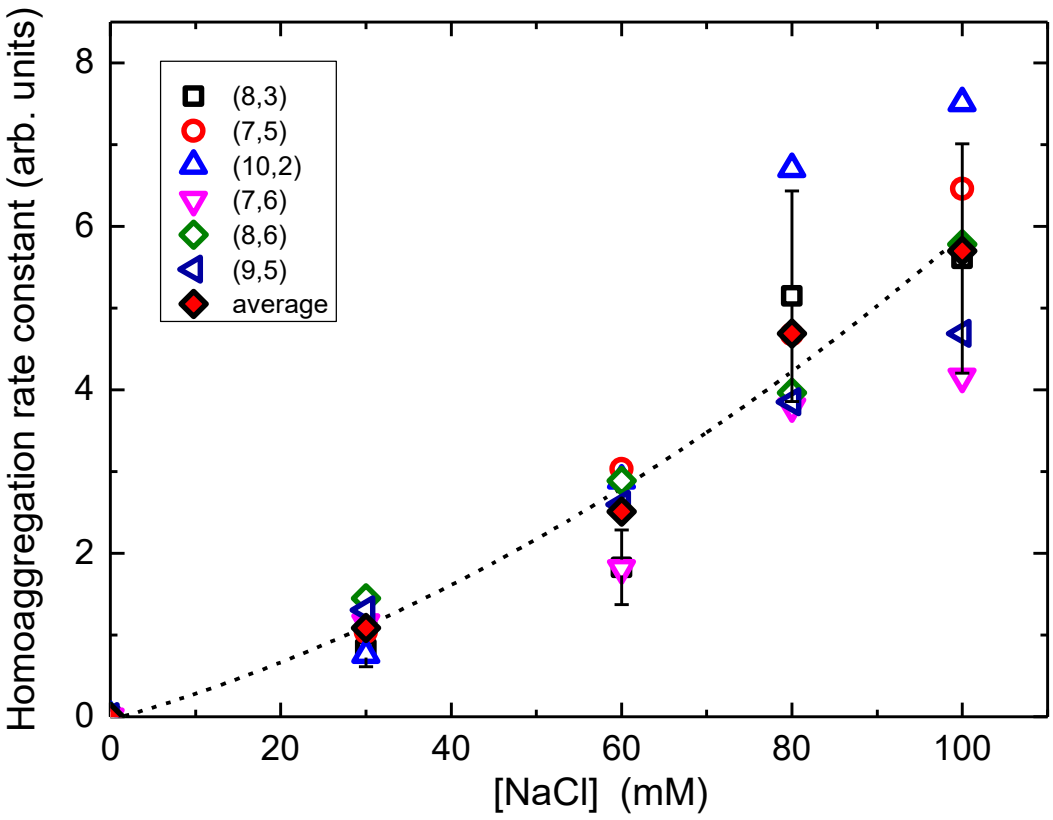

Figure 4. Variation of SWCNT homo-aggregation second-order rate constants as a function of NaCl concentration. Symbols show results for six different (*n*,*m*) species and their average, as computed from initial rates of abundance changes. The error bars show estimated relative uncertainties for all (*n*,*m*) species, and the dashed curve is a guide to the eye.

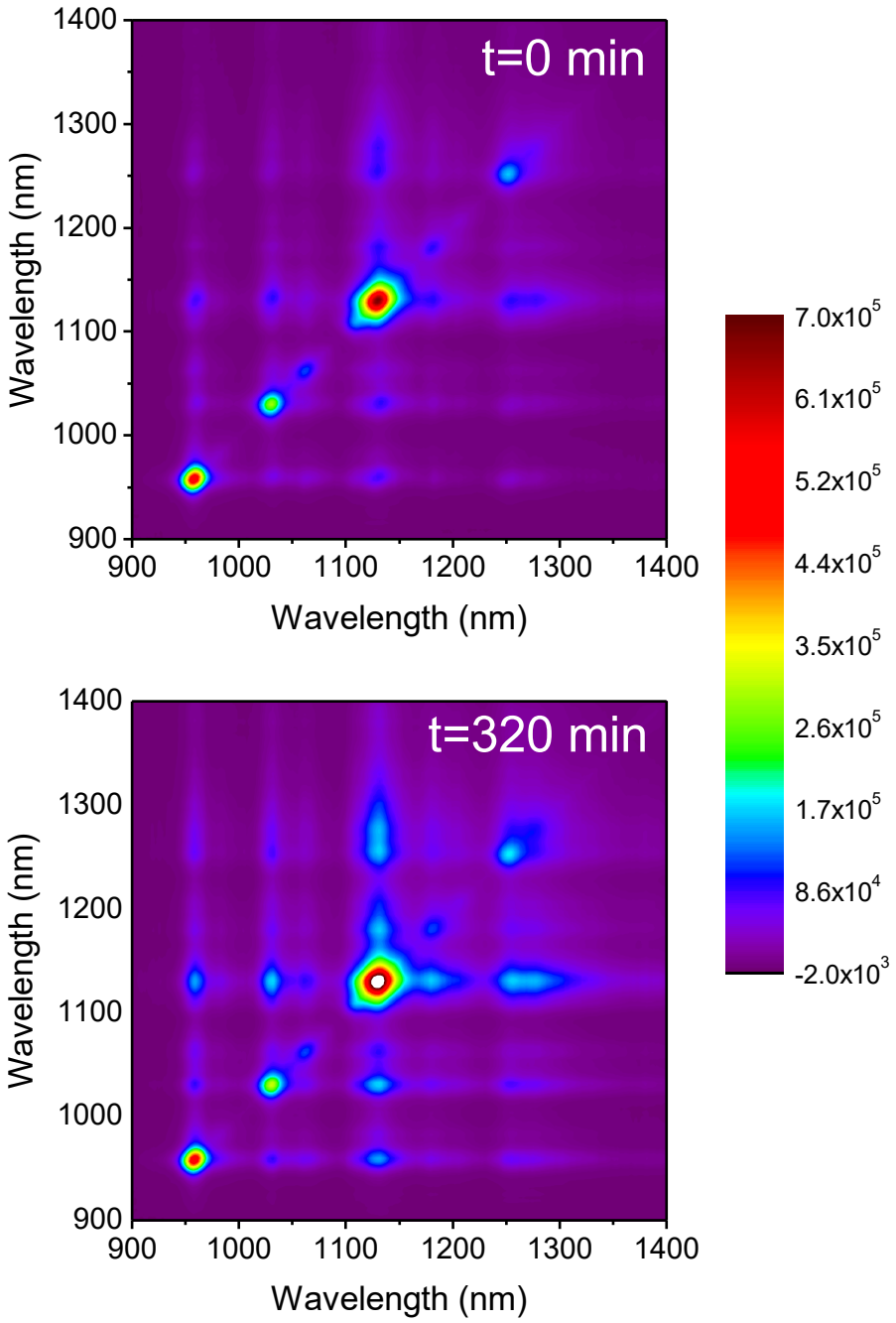

Figure 5. Contour plots of two-dimensional covariance matrices measured from a sample before (top) and 320 min after (bottom) exposure to 30 mM NaCl. Both frames are plotted on the same intensity scale. Pixels with values above 7 x 10^5 appear as white. Intensification of diagonal elements indicates increases in homo-aggregate populations, while intensification of off-diagonal elements indicates increases in hetero-aggregate populations.

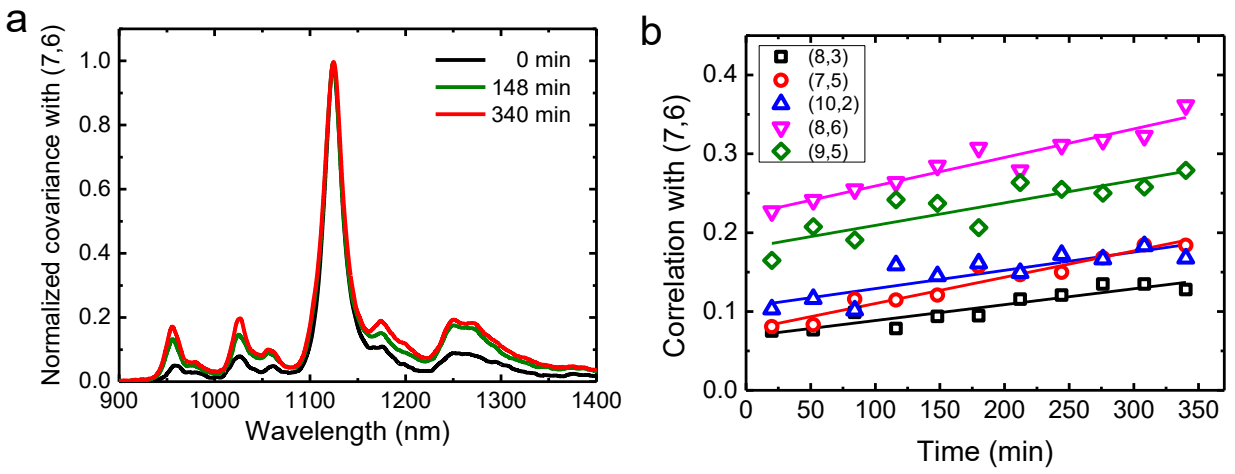

Figure 6. **(a)** Normalized covariance spectra referenced to the (7,6) emission peak measured before and 148 and 340 min after exposure to 30 mM NaCl. Hetero-aggregate formation gives increases in features other than the main peak. **(b)** Computed scaled correlation coefficients after spectral overlap correction, showing fractions of (7,6) particles aggregated with the five other resolved species in the sample. The legend shows (*n*,*m*) species symsuperlinjearbol codes and solid lines are linear fits to the data.

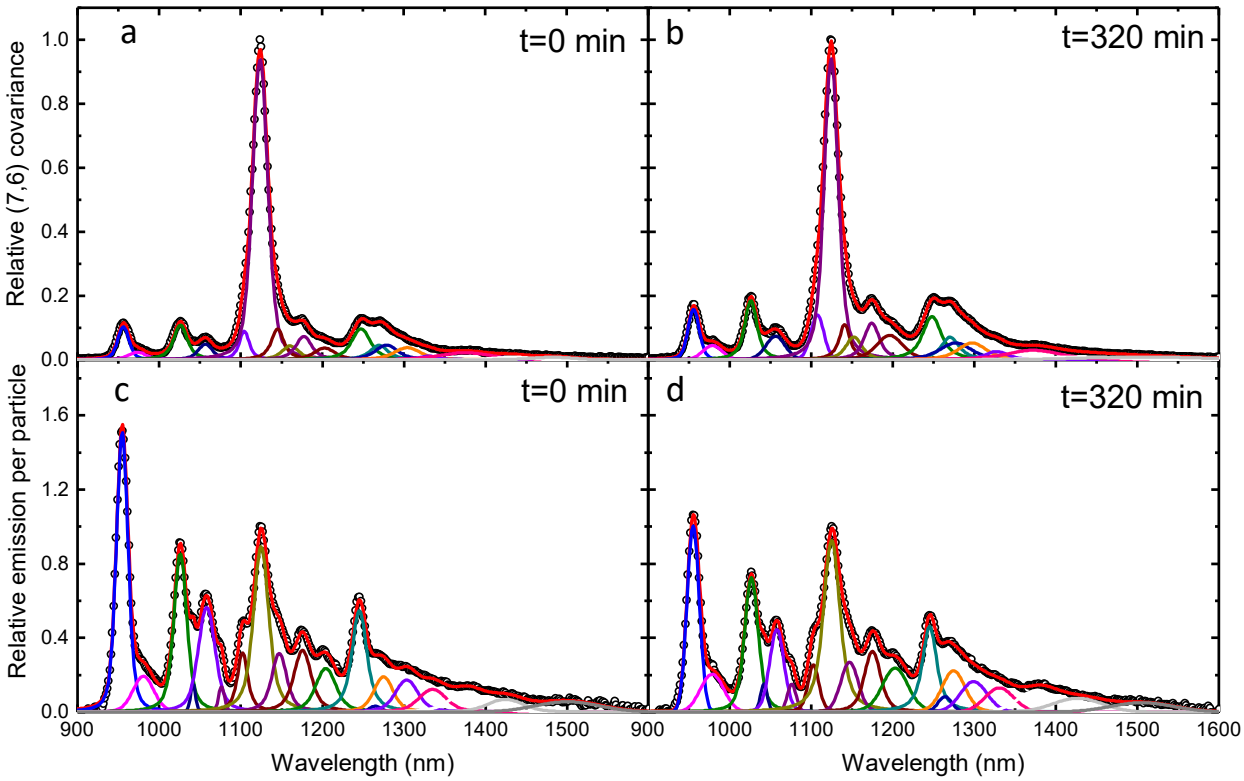

Figure 7. (a), (b) Deconvolution of covariance spectra referenced to the (7,6) emission peak, measured just after and 320 min after exposure to 30 mM NaCl. **(c)**, **(d)** Deconvolution of emission efficiency spectra for the same sample measured for the same times and conditions. In all frames, symbols show experimental data and colored curves show spectral components that add to give the full simulations (red curves).

TOC Graphic

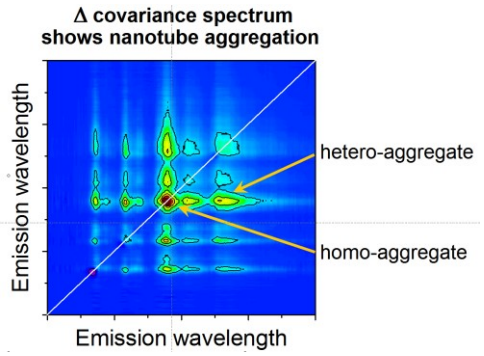
Δ covariance spectrum
shows nanotube aggregation
Emission wavelength
Emission wavelength
hetero-aggregate
homo-aggregate